AMERICAN SOCIETY FOR MICROBIOLOGY | Journal of Virology®

CELLULAR RESPONSE TO INFECTION

The Host Response to Influenza A Virus Interferes with SARS-CoV-2 Replication during Coinfection

Kohei Oishi,[a] Shu Horiuchi,[a] Judith M. Minkoff,[a] Benjamin R. tenOever[a]

[a]Department of Microbiology, New York University, New York, New York, USA

ABSTRACT Severe acute respiratory syndrome coronavirus 2 (SARS-CoV-2) and influenza A virus (IAV) represent two highly transmissible airborne pathogens with pandemic capabilities. Although these viruses belong to separate virus families—SARS-CoV-2 is a member of the family *Coronaviridae*, while IAV is a member of the family *Orthomyxoviridae*—both have shown zoonotic potential, with significant animal reservoirs in species in close contact with humans. The two viruses are similar in their capacity to infect human airways, and coinfections resulting in significant morbidity and mortality have been documented. Here, we investigate the interaction between SARS-CoV-2 USA-WA1/2020 and influenza H1N1 A/California/04/2009 virus during coinfection. Competition assays *in vitro* were performed in susceptible cells that were either interferon type I/III (IFN-I/-III) nonresponsive or IFN-I/-III responsive, in addition to an *in vivo* golden hamster model. We find that SARS-CoV-2 infection does not interfere with IAV biology *in vivo*, regardless of timing between the infections. In contrast, we observe a significant loss of SARS-CoV-2 replication following IAV infection. The latter phenotype correlates with increased levels of IFN-I/-III and immune priming that interferes with the kinetics of SARS-CoV-2 replication. Together, these data suggest that cocirculation of SARS-CoV-2 and IAV is unlikely to result in increased severity of disease.

IMPORTANCE The human population now has two circulating respiratory RNA viruses with high pandemic potential, namely, SARS-CoV-2 and influenza A virus. As both viruses infect the airways and can result in significant morbidity and mortality, it is imperative that we also understand the consequences of getting coinfected. Here, we demonstrate that the host response to influenza A virus uniquely interferes with SARS-CoV-2 biology although the inverse relationship is not evident. Overall, we find that the host response to both viruses is comparable to that to SARS-CoV-2 infection alone.

KEYWORDS anosmia, endemic, H1N1, host response, interference, interferon, long COVID, PASC, pandemic, RNA sequencing

The coronavirus disease 2019 (COVID-19) pandemic, caused by severe acute respiratory syndrome coronavirus 2 (SARS-CoV-2), has resulted in a global health crisis (1, 2). Despite the development of safe and effective vaccines and antiviral drugs, SARS-CoV-2 continues to spread worldwide, with frequent emergence of new viral variants (3–5). SARS-CoV-2 replicates robustly in the upper respiratory tract, inducing inflammation and provoking a range of symptoms including fever, cough, and general malaise (6–8). More severe cases of COVID-19 involve the development of acute respiratory distress syndrome and lung injury, often leading to death. Several risk factors for disease severity have been identified, including sex, age, immunodeficiency, diabetes, and obesity (9–11). In addition, SARS-CoV-2 infection suppresses key components of the innate immune response. More than half of the 30 proteins encoded in the SARS-CoV-2 genome have been reported to counteract interferon (IFN) induction and signaling (12), raising concern about the risk for coinfection with other pathogens.

Several clinical studies have reported coinfection of SARS-CoV-2 with other viruses, including human immunodeficiency virus (HIV), hepatitis B and C viruses (HBV and HCV, respectively),

Editor Mark T. Heise, University of North Carolina at Chapel Hill

Address correspondence to Benjamin R. tenOever, Benjamin.tenOever@NYULangone.org.

The authors declare no conflict of interest.

Received 12 May 2022
Accepted 12 June 2022
Published 12 July 2022

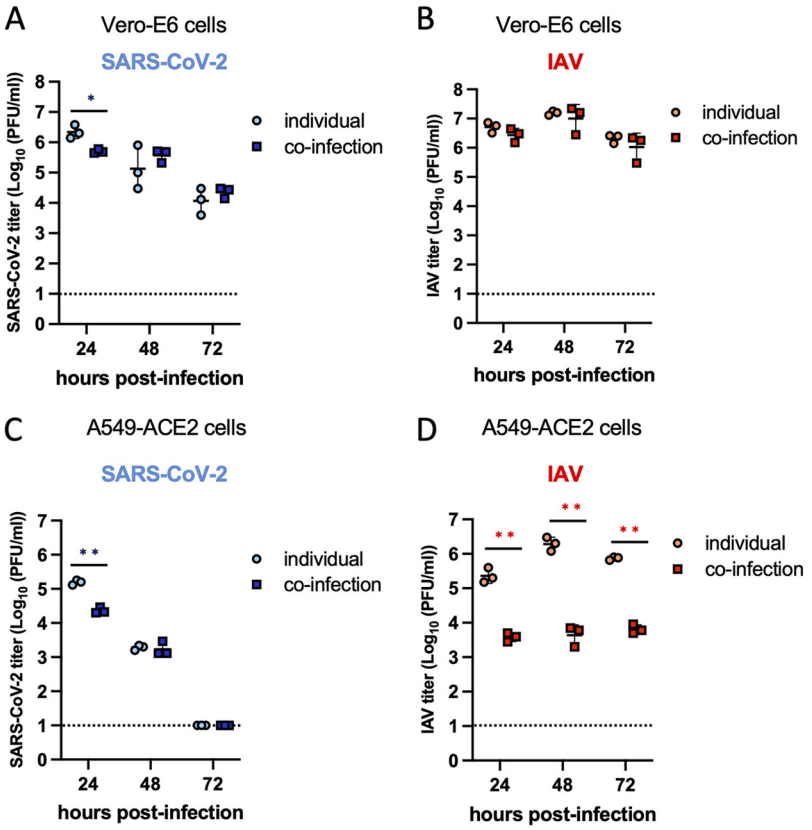

FIG 1 IAV interferes with SARS-CoV-2 replication in cells while SARS-CoV-2 interferes with IAV replication in A549 cells but not Vero-E6 cells. (A and B) Virus titers of SARS-CoV-2 (A) and IAV (B) in individually infected or coinfected Vero-E6 cells. (C and D) Virus titers of SARS-CoV-2 (C) and IAV (D) in individually infected or coinfected A549-ACE2 cells. Cells were infected with SARS-CoV-2 and/or IAV at an MOI of 0.01, and supernatants were collected for plaque assay at 24, 48, and 72 h postinfection (hpi). Virus titers of SARS-CoV-2 and IAV were determined by plaque assay using Vero-E6 cells and MDCK cells, respectively. The dotted line indicates the limit of detection of the plaque assay analysis. *, $P < 0.05$; **, $P < 0.01$.

influenza A and B viruses (IAV and IBV, respectively), and dengue virus (DENV) (13–19). In particular, coinfection with SARS-CoV-2 and IAV was common early in the COVID-19 pandemic, prior to the enforcement of masks and social distancing (17, 20). A meta-analysis of published studies from the first 4 months of the pandemic showed viral coinfection with SARS-CoV-2 in 3% of hospitalized COVID-19 patients, with IAV being among the most common coinfecting viruses (21). Both SARS-CoV-2 and IAV are airborne-transmitted respiratory viruses that can induce acute respiratory distress syndrome. Although these viruses utilize different host receptors for cell entry—SARS-CoV-2 binds to angiotensin-converting enzyme 2 (ACE2) via its spike protein, while human IAV recognizes receptors with saccharides terminating in sialic acid-α2,6-galactose via its hemagglutinin protein (22, 23)—both viruses appear to preferentially infect alveolar type II cells (6, 24).

Here, we investigate the interaction between SARS-CoV-2 and IAV during coinfection *in vitro* and *in vivo* using the golden hamster animal model. Replication kinetics and host responses for animals either simultaneously or sequentially infected with both viruses are described.

RESULTS

Viral replication of SARS-CoV-2 and IAV *in vitro* demonstrates unique patterns of interference. To examine the impact of SARS-CoV-2 and IAV (H1N1 A/California/04/2009) coinfection on viral replication, cells were infected with each virus individually or both at the same time. In Vero-E6 cells that are commonly used for both SARS-CoV-2 and IAV replication studies (25, 26), SARS-CoV-2 exhibited a modest delay in replication in the presence of IAV (Fig. 1A). At 24 h postinfection (hpi), SARS-CoV-2 replicated to lower viral titers in coinfected

cells than it did on its own. However, viral titers were comparable between coinfected and individually infected cells at 48 and 72 hpi (Fig. 1A). In contrast, IAV titers in Vero-E6 cells were unchanged at all time points, regardless of coinfection with SARS-CoV-2 (Fig. 1B).

Given that Vero-E6 cells lack genes encoding type I and III interferons (IFNs), which significantly contribute to viral fitness (27), viral replication was also evaluated in an IFN-competent human lung alveolar cell line. A549 cells are a human alveolar basal epithelial line, commonly used in the study of respiratory infections, including IAV. To allow the evaluation of both IAV and SARS-CoV-2 infection, single-cloned A549-ACE2 cells that express the SARS-CoV-2 entry receptor, human angiotensin-converting enzyme 2, were chosen (28). Cells were infected at a low multiplicity of infection (MOI) with SARS-CoV-2 or IAV alone or with the two viruses together. For SARS-CoV-2, a similar trend was observed in A549-ACE2 as in Vero-E6 cells. SARS-CoV-2 replication was lower in the presence of IAV at 24 hpi but comparable at 48 hpi (Fig. 1C). In contrast to the viral kinetics observed in Vero-E6 cells, IAV viral titers were substantially lower in the presence of SARS-CoV-2 in A549-ACE2 cells at all time points (Fig. 1D). Taken together, these results suggest that IAV coinfection may contribute to a delay in SARS-CoV-2 replication in both Vero-E6 and A549-ACE2 cells. In contrast, SARS-CoV-2 coinfection appears to significantly interfere with IAV replication in interferon-competent A549-ACE2 cells but not in interferon-defective Vero-E6 cells.

IAV interferes with SARS-CoV-2 replication in coinfected hamsters. The golden hamster model represents a robust system for studying both SARS-CoV-2 and IAV, due to its ability to recapitulate the pathological and immunological characteristics of disease in humans (26, 29–32). Inoculation of hamsters with either IAV or SARS-CoV-2 results in robust replication in the respiratory tract and induces both innate and adaptive immune responses (8, 26, 30, 32). To assess the host response to individual infection and coinfection with both viruses, hamsters were intranasally infected with SARS-CoV-2, IAV, or both viruses simultaneously (Fig. 2A). Virus titers of SARS-CoV-2 and IAV in the lungs at 1, 3, 5, 7, and 14 days postinfection (dpi) were determined by plaque assay. Each virus replicated robustly in the respiratory tracts of the hamsters, exhibiting peak titers at 3 dpi in individually infected animals (Fig. 2B and C). In coinfected hamsters, SARS-CoV-2 lung titers were comparable to those of individually infected hamsters at 1 dpi; however, these animals exhibited lower SARS-CoV-2 titers at 3 dpi and rapid SARS-CoV-2 clearance in the lung by 5 dpi. In contrast, infectious virus particles were detected in 100% of the SARS-CoV-2 individually infected hamsters at 5 dpi and 25% at 7 dpi (Fig. 2B). IAV titers in the lungs were not impacted by SARS-CoV-2 coinfection at any time point tested (Fig. 2C). These data suggest that IAV and SARS-CoV-2 coinfection in hamsters is associated with lower levels of SARS-CoV-2 replication but no change in IAV replication. Coinfected animals, or those challenged with SARS-CoV-2 alone, showed a delayed lack of weight gain compared to phosphate-buffered saline (PBS)-treated or IAV-infected hamsters (Fig. 2D). These differences in morbidity could also be observed in lung histology, as coinfection or animals infected with SARS-CoV-2 each showed extensive infiltration of mononuclear cells by hematoxylin and eosin (H&E) stain, indicative of immune cell infiltration (Fig. 2E).

In an effort to better understand the immune response to individual infection and coinfection in hamsters, we performed mRNA sequencing (mRNA-seq) to evaluate differential gene expression (DGE) in the respiratory tract at 5 dpi (Fig. 2F and G). Our group previously found that SARS-CoV-2 infection induces a more pronounced inflammatory signature in hamsters than IAV, which is consistent with what has been observed in COVID-19 patients and in the ferret model (8, 26, 31). Coinfection with SARS-CoV-2 and IAV also produced a more robust inflammatory response than did infection with IAV alone (Fig. 2F). These data indicate that the host response to SARS-CoV-2 or coinfection includes the same genes induced by IAV in addition to others as indicated in the volcano plots (Fig. 2F and G). SARS-CoV-2-specific genes showed an enrichment in NF-κB-dependent chemokines such as CCL2, CCL5, CCL7, and CXCL10, in agreement with other published work (Table 1) (33). These results suggest that the host response to SARS-CoV-2 would induce much greater immune infiltration given the chemokine expression which is corroborated by the H&E stains (Fig. 2E).

Preinfection of hamsters with IAV suppresses SARS-CoV-2 replication, but preinfection with SARS-CoV-2 does not impact the growth of IAV. To further examine the dynamics between SARS-CoV-2 and IAV biology, hamsters were mock treated or preinfected with

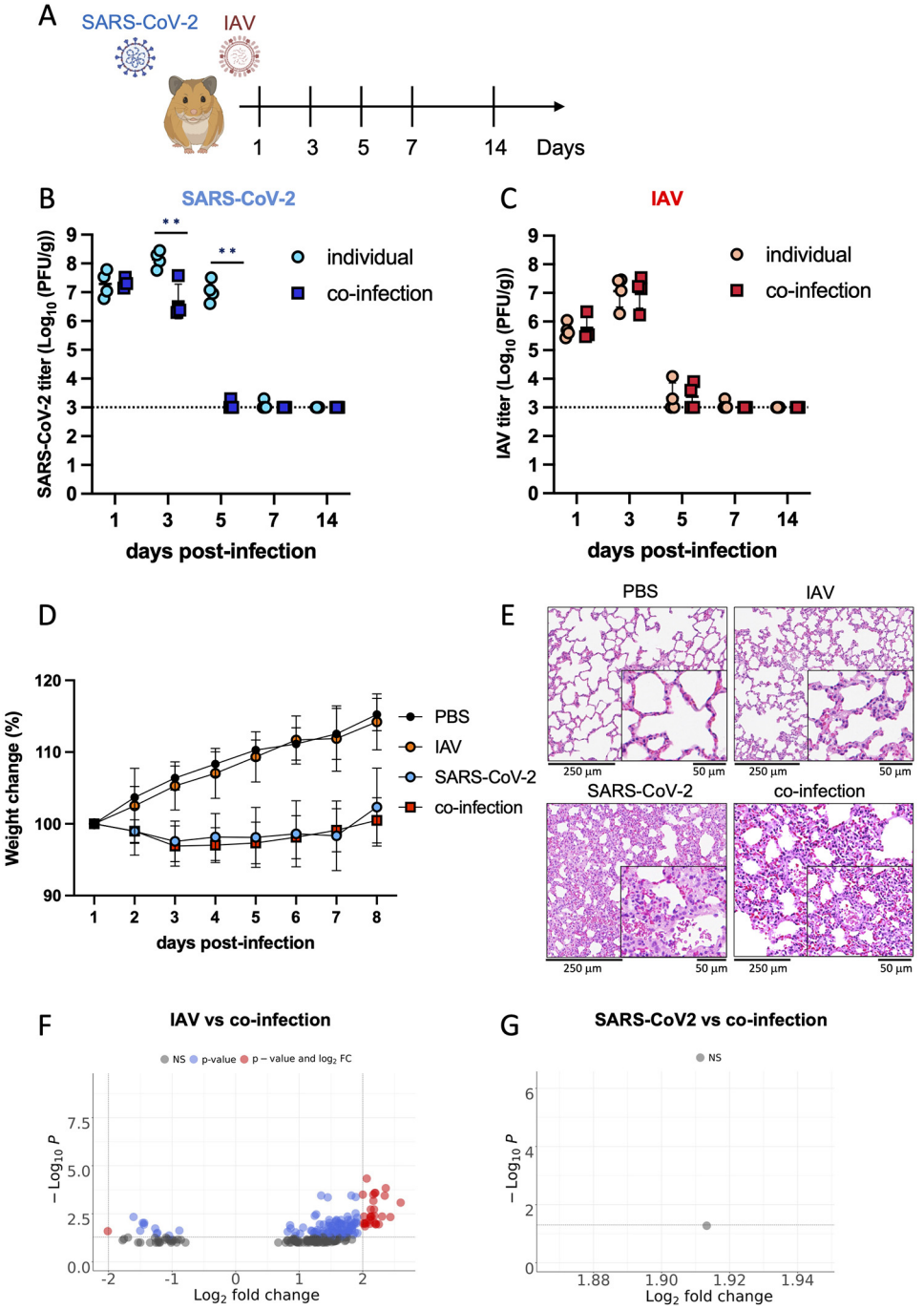

FIG 2 IAV interferes with SARS-CoV-2 replication in coinfected hamsters. (A) Experimental protocol of hamster infection. Six- to 8-week-old golden hamsters were intranasally inoculated with either 10^3 PFU of SARS-CoV-2, 10^5 PFU of IAV, or both viruses simultaneously ($n = 4$, at each time point). Lungs were collected at 1, 3, 5, 7, and 14 days postinfection (dpi) for virus titer and gene expression analysis. (B and C) Virus titers of SARS-CoV-2 (B) and IAV (C) in the lungs of hamsters individually infected or coinfected with each virus. Lungs were harvested for plaque assay at 1, 3, 5, 7, and 14 dpi. *, $P < 0.05$; **, $P < 0.01$. The dotted line indicates the limit of detection of the plaque assay analysis. (D) Body weight change in hamsters after infection. Hamsters were intranasally inoculated with either PBS, 10^3 PFU of SARS-CoV-2, 10^5 PFU of IAV, or both viruses simultaneously. Data are presented as a mean percentage of the starting weight. Eight hamsters per condition are shown. (E) Representative histopathology images of the lungs of hamsters inoculated with either PBS, 10^3 PFU of SARS-CoV-2, 10^5 PFU of IAV, or both viruses simultaneously. Lungs were fixed and stained with hematoxylin and eosin (H&E) at 3 dpi. (F and G) Volcano plot comparing DEGs in the lungs of hamsters individually infected or coinfected with IAV and/or SARS-CoV-2 at 5 dpi (gray, not significant [NS]; blue, significant; red, significant and $\log_2$ fold change of >2).

TABLE 1 Differentially expressed genes showing a $\log_2$ fold change of 2 or greater in comparison of IAV-infected and coinfected hamsters at 5 dpi

Hamster gene identifier	Human orthologue	Log_2FC	*P* value
ENSMAUG00000000889	SCYL3	2.597016633	1.71E−06
ENSMAUG00000014152	JCHAIN	2.435561429	2.00E−05
ENSMAUG00000000781	ADAMTS4	2.361910532	4.65E−08
ENSMAUG00000010986	IL1RN	2.345971382	5.15E−07
ENSMAUG00000021684	CCL2	2.304400759	1.66E−05
ENSMAUG00000021354	CCL7	2.253364797	9.71E−05
ENSMAUG00000016429	UBE2L6	2.208360031	9.04E−05
ENSMAUG00000012996	GDF15	2.204550607	0.00010683
ENSMAUG00000013200	ANGPTL4	2.199003285	1.54E−07
ENSMAUG00000019004	TIMP1	2.188953832	1.65E−07
ENSMAUG00000014450	CXCL10	2.187217601	5.93E−05
ENSMAUG00000017767	TLDC2	2.18320049	1.19E−05
ENSMAUG00000014385	IL18BP	2.17778203	4.35E−06
ENSMAUG00000015793	SOCS1	2.167451672	1.28E−06
ENSMAUG00000010396	CCL5	2.165689727	3.03E−07
ENSMAUG00000002531	SLAMF9	2.141679697	1.67E−05
ENSMAUG00000010793	DUSP2	2.125972291	4.47E−06
ENSMAUG00000000191	GZMB	2.125334416	1.56E−05
ENSMAUG00000016341	FCGR3A	2.122718258	1.84E−05
ENSMAUG00000018138	APOBEC1	2.114941777	3.46E−05
ENSMAUG00000013142	LAG3	2.113133581	8.31E−05
ENSMAUG00000017709	UPP1	2.063067423	7.37E−09
ENSMAUG00000009013	OGFR	2.061656232	6.23E−05
ENSMAUG00000016807	IRF7	2.036182613	0.00015812
ENSMAUG00000001396	IL21R	2.033723293	7.01E−05
ENSMAUG00000018825	TM4SF19	2.033399608	9.14E−05
ENSMAUG00000012209	DUSP5	2.021127846	1.60E−05
ENSMAUG00000012044	COA7	2.007215953	7.91E−05
ENSMAUG00000021487	ARID5A	2.000914165	2.91E−07

either SARS-CoV-2 or IAV and then challenged with the other virus (Fig. 3A to F). To measure the effect of IAV preinfection on SARS-CoV-2 replication, hamsters were inoculated with PBS or IAV, and after 3 days, they were treated again with PBS or infected with SARS-CoV-2 (Fig. 3A). Hamsters that were preinfected with IAV generated lower SARS-CoV-2 virus titers than did their SARS-CoV-2 individually infected counterparts at each time point, indicating IAV preinfection is associated with reduced SARS-CoV-2 replication, corroborating the direct coinfection (Fig. 2B and Fig. 3B). In contrast, IAV titers were not changed by SARS-CoV-2 infection during active IAV replication in hamsters (Fig. 3C).

Next, to look at the effect of SARS-CoV-2 preinfection on IAV replication, a separate group of hamsters was inoculated with PBS or SARS-CoV-2 followed by a second inoculation of PBS or IAV 3 days afterward (Fig. 3D). SARS-CoV-2 preinfection did not affect IAV replication (Fig. 3E). Despite the observation that IAV coinfection and preinfection were associated with decreased SARS-CoV-2 replication (Fig. 2B and Fig. 3B), SARS-CoV-2 titers were not changed by later infection with IAV (Fig. 3F). Taken together, these data suggest that IAV preinfection may interfere with SARS-CoV-2 growth but that SARS-CoV-2 preinfection does not impact the replication of IAV. Furthermore, no delays in virus clearance were observed in hamsters infected with either SARS-CoV-2 or IAV and preinfected with the other virus.

IAV infection reduces SARS-CoV-2 replication even after IAV clearance. Based on the observation that IAV coinfection and preinfection are associated with reduced SARS-CoV-2 replication in hamsters, we examined the effect of SARS-CoV-2 infection on a cohort of IAV-recovered hamsters (Fig. 4A and C). At 7 days after IAV infection, a time point where no infectious material is detectable (Fig. 1B), hamsters were challenged with SARS-CoV-2 (Fig. 4A). Despite evidence that IAV was cleared at this time point, SARS-CoV-2 titers in IAV-recovered hamsters remained lower at 1 and 3 dpi than in hamsters preinoculated with PBS and reached comparable levels only at 5 dpi with SARS-CoV-2, and SARS-CoV-2

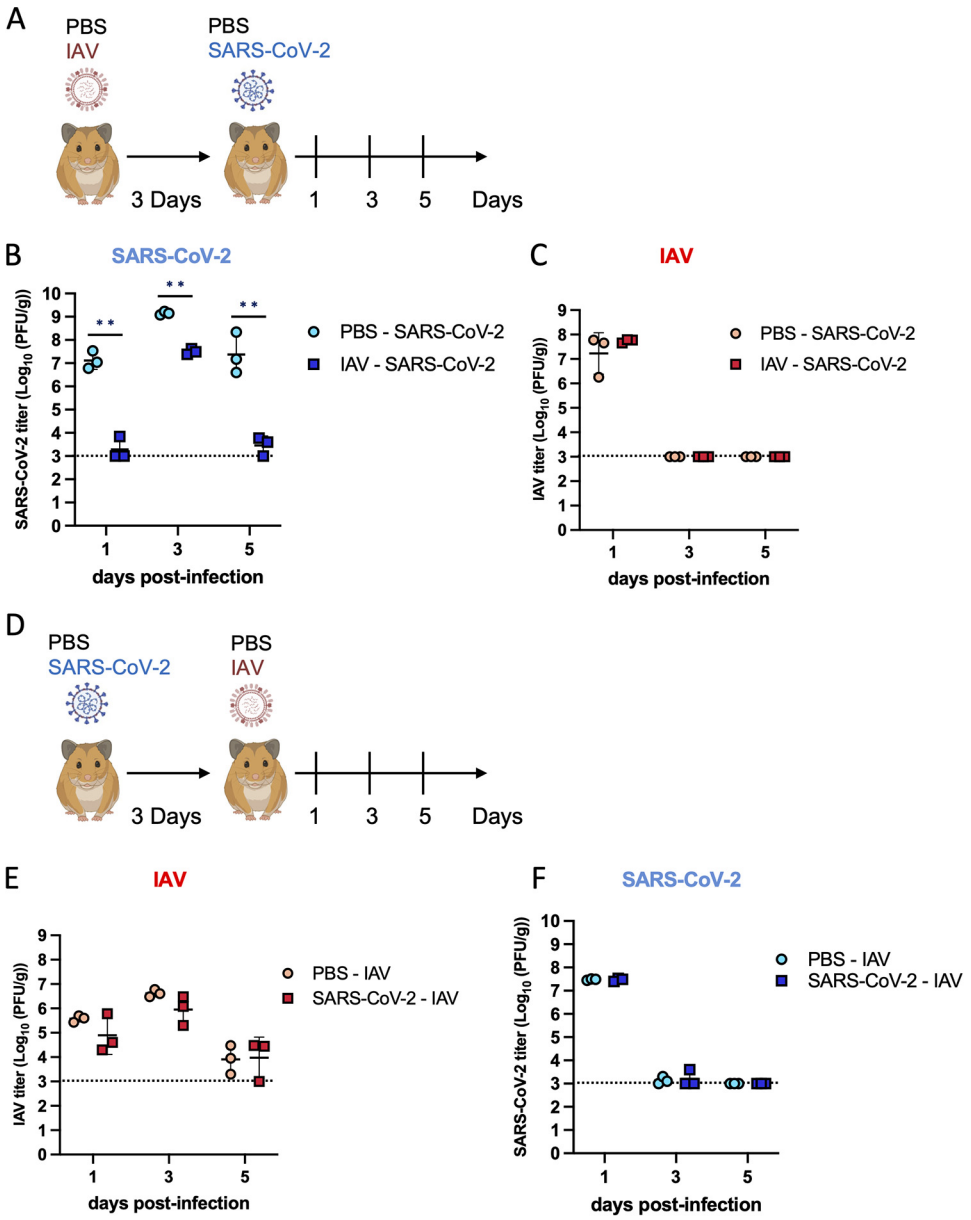

FIG 3 Preinfection by IAV suppresses SARS-CoV-2 replication, but preinfection by SARS-CoV-2 does not impact IAV growth. (A) Experimental protocol of hamster preinfection. Golden hamsters were intranasally inoculated with either PBS or 10^5 PFU of IAV. At 3 dpi, hamsters were inoculated with PBS or 10^3 PFU of SARS-CoV-2 (n = 3, at each time point). (B and C) Virus titers of SARS-CoV-2 (B) and IAV (C) in the respiratory tract at each time point. ** indicates $P < 0.01$. The dotted line indicates the limit of detection of the plaque assay analysis. (D) Experimental protocol of hamster preinfection. Golden hamsters were intranasally inoculated with either PBS or 10^5 PFU of IAV on day 3 after PBS treatment or infection with 10^3 PFU of SARS-CoV-2 (n = 3, at each time point). (E and F) Virus titers of IAV (E) and SARS-CoV-2 (F) in hamster lungs at each time point were determined by plaque assay. The dotted line indicates the limit of detection of the plaque assay analysis.

was not detected at 7 dpi in both cohorts (Fig. 4B). To extend the observation to a later time after infection with IAV, we again challenged IAV-recovered hamsters with SARS-CoV-2, this time allowing the animals 2 weeks to fully recover from the initial treatment (Fig. 4C). Even at this time point, SARS-CoV-2 titers were lower at 1 dpi than in PBS-treated SARS-CoV-2-infected hamsters (Fig. 4D). These results suggest that IAV infection results in changes to biology of the airways in a manner that influences the initial rate of SARS-CoV-2 replication. SARS-CoV-2 infection in hamsters harboring IAV showed low peak titers and rapid clearance of SARS-CoV-2, while SARS-CoV-2 infection in IAV-recovered hamsters demonstrated a loss of early SARS-CoV-2 replication (Fig. 2B and Fig. 3B). These data suggest that the gene

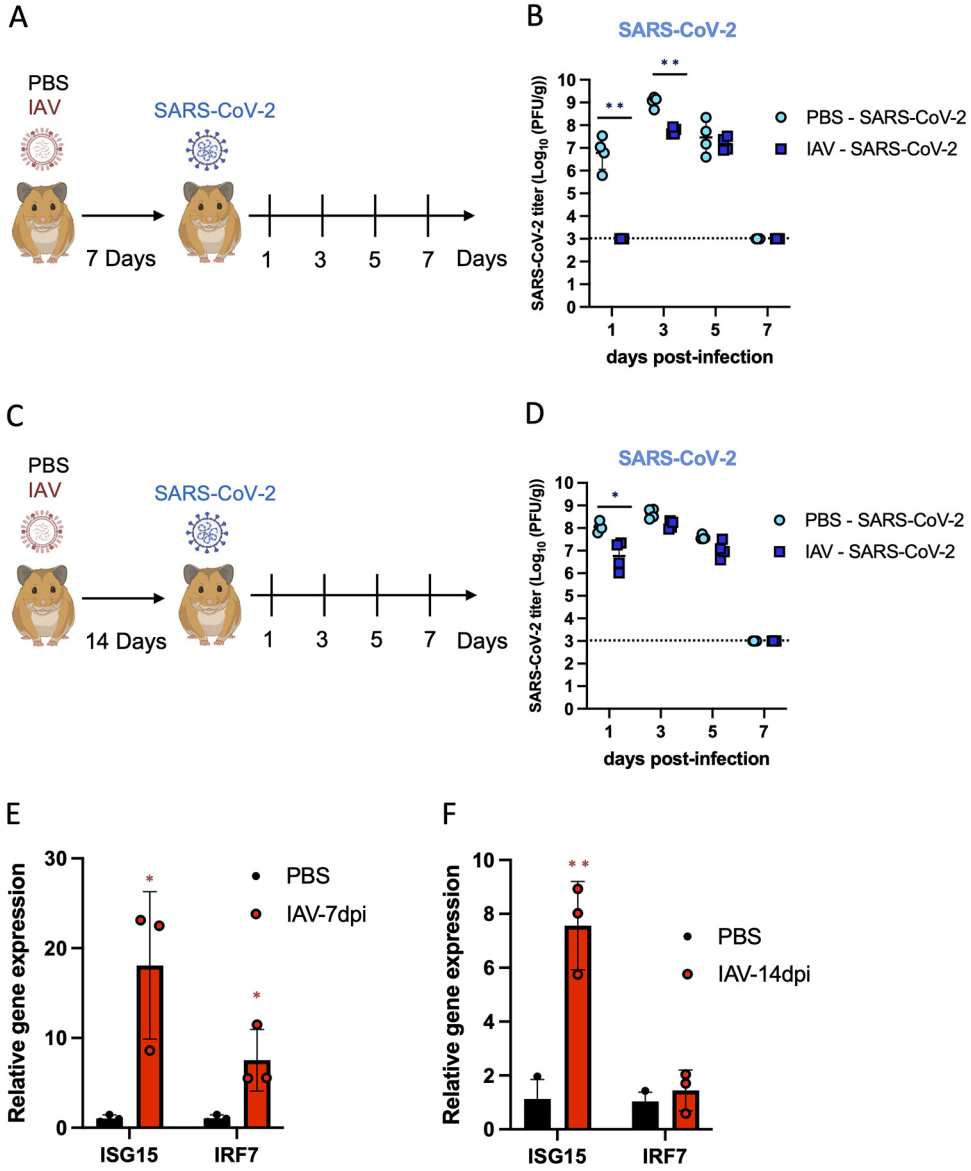

FIG 4 IAV interferes with SARS-CoV-2 replication even after IAV clearance. (A) Experimental protocol of infection in IAV-recovered hamsters. Golden hamsters were intranasally inoculated with either PBS or 10^5 PFU of IAV. At 7 dpi, hamsters were infected with 10^3 PFU of SARS-CoV-2. Lung tissues were collected at 1, 3, 5, and 7 days after SARS-CoV-2 infection for virus titer ($n = 4$, at each time point). (B) SARS-CoV-2 titers in the respiratory tract at 1, 3, 5, and 7 days after infection with SARS-CoV-2. ** indicates $P < 0.01$. The dotted line indicates the limit of detection of the plaque assay analysis. (C) Experimental protocol of infection in IAV-recovered hamsters. Golden hamsters were intranasally infected with 10^3 PFU of SARS-CoV-2 on day 14 after inoculation with either PBS or 10^5 PFU of IAV. (D) Virus titers of SARS-CoV-2 in hamster lungs at 1, 3, 5, and 7 days after infection with SARS-CoV-2. * indicates $P < 0.05$. The dotted line indicates the limit of detection of the plaque assay analysis. (E and F) mRNA expression level of *ISG15* and *IRF7* represented by RT-qPCR. Total RNA isolated from the lungs of PBS-treated or IAV-infected hamsters at 7 or 14 days after inoculation was assessed for gene expression by quantitative real-time PCR using beta-actin-, *ISG15*-, and *IRF7*-specific primers. Delta-delta cycle threshold was determined relative to PBS-treated samples. Error bars denote standard deviation across samples ($n = 3$). *, $P < 0.05$; **, $P < 0.01$.

expression and environment in the respiratory tract at the different time points after IAV infection contribute to the kinetics of SARS-CoV-2 biology.

To explore the mechanism by which IAV infection interferes with SARS-CoV-2 replication in hamsters, we performed mRNA-seq at 7 days after PBS treatment or IAV infection to evaluate differential gene expression in the respiratory tract that be responsible for the delayed replication of SARS-CoV-2. These data, which represent cohorts of hamsters treated with only PBS or infected with IAV for 7 days, demonstrated only 25 differentially expressed genes (DEGs), suggesting that the host response to IAV had largely returned to baseline (Table 2).

TABLE 2 Differentially expressed genes between PBS-treated and IAV-infected hamsters at 7 dpi

Hamster gene ID	Human orthologue	Log_2FC	*P* value
ENSMAUG00000000889	RAB7B	0.99806831	2.15E−06
ENSMAUG00000014152	JCHAIN	0.96543212	1.68E−06
ENSMAUG00000000781	CCL5	0.94312191	1.44E−06
ENSMAUG00000010986	C1QC	0.92851863	1.02E−05
ENSMAUG00000021684	FBLN2	0.87133358	1.15E−05
ENSMAUG00000021354	TRF	0.86261419	4.24E−05
ENSMAUG00000016429	C1QB	0.85178249	3.44E−05
ENSMAUG00000012996	C1QA	0.83651579	5.31E−05
ENSMAUG00000013200	ARPP19	0.82299565	8.26E−05
ENSMAUG00000019004	IGHV4	0.82293325	3.08E−05
ENSMAUG00000014450	IGKV6	0.81852337	1.36E−06
ENSMAUG00000017767	ELN	0.80290137	1.05E−06
ENSMAUG00000014385	LY6E	0.78623131	0.0001202
ENSMAUG00000015793	SCYL3	0.77811553	5.34E−05
ENSMAUG00000010396	RARRES2	0.72304586	3.05E−05
ENSMAUG00000002531	SLAMF9	0.70778807	1.95E−05
ENSMAUG00000010793	LAG3	0.5702712	0.0001389
ENSMAUG00000000191	PTP4A1	0.52076904	1.83E−05
ENSMAUG00000016341	IGHG3	0.50248798	5.04E−06
ENSMAUG00000018138	SPP1	0.23402256	2.49E−05
ENSMAUG00000013142	CD177	0.23371347	5.17E−05
ENSMAUG00000017709	PLVAP	−0.7153702	1.39E−05
ENSMAUG00000009013	HAX1	−1.1209636	9.41E−09
ENSMAUG00000016807	CCDC141	−1.2270713	5.12E−09
ENSMAUG00000001396	PED1B	−1.3570871	2.64E−11

Among the genes that were modestly enriched (log_2 fold change [L2FC] between 0.8 and 1), we did observe a low level of immune priming (GO:0050778, LAG3, PCED1B, and CCL5m IGJ) as well as evidence for increased levels of macrophages based on the enrichment of C1QA, C1QB, C1QC, ARPP19, and RAB7B (Table 2). To further assess specific gene expression related to a priming of the host antiviral response, the expression of key genes involved in the type I IFN response (*ISG15* and *IRF7*) was evaluated by quantitative real-time PCR (RT-qPCR). Both *ISG15* and *IRF7* were highly expressed in the lungs at 7 dpi, and elevated *ISG15* expression was observed until 14 dpi (Fig. 4E and F). These data suggest the possibility that the type I IFN response induced by IAV infection may remain at a low level after viral clearance or may result in an increase in resident immune cells in the airways—either of which would contribute to the reduction of SARS-CoV-2 replication.

DISCUSSION

Clinical reports from several regions have warned of the risk of SARS-CoV-2 and IAV coinfection (34–37). Given the extensive global spread of SARS-CoV-2 and the relaxation of pandemic restrictions, there is a strong potential for SARS-CoV-2 and IAV coinfection to become common, as it was early in the COVID-19 pandemic, prior to the enforcement of masks and social distancing (17). The data presented here help to shed light on the interaction between SARS-CoV-2 and IAV in coinfected hosts. Using the golden hamster model, we find that IAV interferes with SARS-CoV-2 replication in the lung, even more than 1 week after IAV clearance. In contrast, IAV exhibited robust replication in the respiratory tract of hamsters, regardless of the presence of SARS-CoV-2. These data suggest the presence of factors intrinsic to or induced by IAV that may restrict the growth of SARS-CoV-2, but it remains unclear whether this effect plays a role in disease severity.

Experimental studies using hamsters and K18-hACE2 transgenic mice have examined the influence of coinfection on virus replication and disease severity (38–41). In K18-hACE2 mice, coinfection with SARS-CoV-2 and IAV resulted in increased disease severity, and both preinfection and coinfection with IAV resulted in higher SARS-CoV-2 viral loads in the lungs and nasal turbinate and delayed viral clearance (38, 39, 42). SARS-CoV-2 and IAV coinfection also

resulted in increased disease severity compared to single infection in golden hamsters; however, unlike in the mouse model, coinfected hamsters exhibited lower SARS-CoV-2 viral loads in the lungs (41), similar to what was observed in the present study. Despite this phenotype, SARS-CoV-2 shedding lasted longer in coinfected hamsters (41). In contrast, coinfection by SARS-CoV-2 and H3N2 IAV of female hamsters results in robust SARS-CoV-2 virus replication but low IAV titers (40). Although we did not observe extended viral shedding of SARS-CoV-2 or suppression of IAV replication in coinfected animals, it is possible that the impact of coinfection on the replication and pathogenicity of each virus is somewhat dependent on other factors such as sex, age, and/or virus strain (40, 41). Further experiments using barcoded viruses would aid in discerning more of the molecular mechanisms responsible for virus interference by the same or different virus strains (43).

Although SARS-CoV-2 and IAV utilize unique receptors for infection, ACE2 and sialic acid-α2,6-galactose (22, 23), respectively, respiratory epithelial cells such alveolar type II cells can be infected with both viruses (6, 24). We observed a significant loss of SARS-CoV-2 replication following IAV infection; however, it is still unclear if the inhibition of replication is due to direct effects in coinfected cells or bystander events on neighboring cells. As IAV infection suppressed SARS-CoV-2 early replication even after clearance (Fig. 4), the phenotype described here is likely the product of immune priming with IFN-I/-III. Although antibodies to cell markers are limited in the hamster model, future single-cell sequencing efforts could resolve whether viral interference is also the product of direct coinfection.

Here, we show that IAV interferes with SARS-CoV-2 both *in vitro* and *in vivo* through a mechanism involving both an IFN-I-dependent and an IFN-I-independent mechanism. In contrast, SARS-CoV-2 infection appears to interfere only with subsequent IAV spread in IFN-competent cells, suggesting SARS-CoV-2 may have a more difficult time controlling the host response than IAV. This same experimental setup in hamsters, which are IFN competent, did not show this phenotype, presumably because the lung provides an expansive cellular landscape for infection and includes many specialized cell types that can modulate the host response that would not be phenocopied using *in vitro* cultures. While the presented *in vitro* data are informative, the *in vivo* results illustrate the physiological manifestation of how these dynamics truly play out in the context of a *de novo* infection.

We also demonstrate that IAV-recovered hamsters still maintained elevated gene expression of the IFN-stimulated genes *IRF7* and *ISG15* until 7 dpi and 14 dpi, respectively (Fig. 4E and F), suggesting the innate immune response following IAV infection could partially contribute to the reduction of SARS-CoV-2 replication in these animals. On the other hand, coinfection or preinfection by SARS-CoV-2 did not change IAV titers in hamsters (Fig. 2C and Fig. 3C), suggesting that IAV may be able to replicate well even in an IFN-I-primed environment given a sufficient number of susceptible cells. Another contributing factor to the observed phenotype could be the kinetics by which the host response is induced following either SARS-CoV-2 or IAV infection. Earlier reports leveraging the hamster model in response to these same strains of SARS-CoV-2 and IAV do provide additional support for this concept (26). For example, in response to IAV, Horiuchi et al. demonstrated that peak interferon-stimulated gene (ISG) and chemokine levels in the airways were evident at 3 dpi and diminished thereafter (26). In contrast, the host response to SARS-CoV-2 lagged behind that to IAV but was more prolonged, with peak ISGs and chemokines observed from 5 to 7 dpi (26, 31). These dynamics would suggest that the unique host response to different viruses can contribute to the interference of one virus over another during coinfection. Elucidating the molecular mechanism(s) underlying this biology will require additional work and is likely to be influenced by both the virus family and/or strain. For example, others have investigated the role of IFN-stimulated genes during SARS-CoV-2 and IAV coinfection. In the golden hamster model, Mx1 was implicated in the inhibition of IAV replication during coinfection and preinfection with SARS-CoV-2, whereas no inhibition was seen in the reverse scenario (40). In our study, SARS-CoV-2 infection did not impact the replication of IAV in hamsters despite robust induction of Mx1, which we have demonstrated elsewhere (31, 32). As previously noted, it is possible that different strains used for infection could impact the expression of certain antiviral genes; however, based on earlier work from our group, it seems that Mx1 induction in response to SARS-CoV-2 is more

evident in tissues that are not productively infected and is delayed in the airways (31). These disparate results may also be due to different viral strains utilized (40). However, regardless of whether SARS-CoV-2 can also interfere with IAV biology, these studies clearly demonstrate that coinfection dynamics can be very complex as a result of the host response and can lead to unpredictable outcomes in relation to disease.

MATERIALS AND METHODS

Hamsters. Male Syrian golden hamsters were purchased from Charles River Laboratories and housed in a temperature-controlled environment with 12 h of light per day at the Center for Comparative Medicine and Surgery (CCMS) at the Icahn School of Medicine at Mount Sinai (New York, NY, USA). All experiments involving viral infections were carried out in a CDC/USDA-approved biosafety level 3 (BSL-3) facility at CCMS, and animals were transferred into the facility a minimum of 7 days prior to onset of experiments. All experimental procedures and the protocol were approved by the Institutional Animal Care and Use Committee at the Icahn School of Medicine at Mount Sinai (IACUC-2016-0438). Six- to 8-week-old hamsters were anesthetized by intraperitoneal injection with 200 μL of a ketamine-xylazine solution (3:1) (100 mg/kg of body weight). Each animal was inoculated intranasally with 100 μL of PBS, 10^3 PFU of SARS-CoV-2, 10^5 PFU of IAV, or 10^3 PFU of SARS-CoV-2 and 10^5 PFU of IAV. Hamsters were euthanized by intraperitoneal injection of pentobarbital. Lung tissues were fixed for histological analysis or homogenized in lysing matrix A homogenization tubes (MP Biomedicals) in a FastPrep-24 5G bead-beating grinder and lysis system (MP Biomedicals). Lungs for plaque assay were homogenized with an amount of PBS according to their weight. For RNA isolation, lung tissues were homogenized with 1 mL of TRIzol (Invitrogen).

Cells. Human adenocarcinomic alveolar basal epithelial (A549) cells (ATCC, CCL-185), African green monkey kidney epithelial Vero-E6 cells (ATCC, CRL-1586), and Madin-Darby canine kidney (MDCK) cells (ATCC, CRL-2935) were maintained at 37°C and 5% CO_2 in Dulbecco's modified Eagle's medium (DMEM; Gibco) supplemented with 10% fetal bovine serum (FBS; Corning). All cell were analyzed to ensure they were mycoplasma free on a biweekly basis. A549-ACE2 cells were generated by transducing A549 cells with a lentivirus encoding human ACE2. After puromycin selection, a single clone was isolated and expanded.

Viruses. Severe acute respiratory syndrome coronavirus 2 (SARS-CoV-2) isolate USA-WA1/2020 (NR-52281) was deposited by the Centers for Disease Control and Prevention and obtained through BEI Resources, NIAID, NIH. SARS-CoV-2 and influenza A virus (IAV) (pdmH1N1 A/California/04/2009) were propagated in Vero-E6 cells in DMEM supplemented with 5% FBS or in MDCK cells in Eagle's minimum essential medium (EMEM; Gibco) supplemented with 3% bovine serum albumin (BSA) and 1 μg/mL tosylsulfonyl phenylalanyl chloromethyl ketone (TPCK)-trypsin, respectively. Virus stocks were characterized using plaque assay and RNA sequencing to ensure genome integrity and infectivity. Infectious titers of SARS-CoV-2 or IAV were determined by plaque assay using 100 μL of supernatant or lung homogenates in Vero-E6 cells or MDCK cells, respectively. Limits of detection of plaque assay of cell and animal experiments are $\log_{10} = 1$ PFU/mL and $\log_{10} = 3$ PFU/g, respectively.

Histological analysis. Lung tissues were harvested and fixed in 10% neutral buffered formalin for 24 to 48 h. Fixed tissues were then embedded in paraffin and sectioned for analysis. Each slide was deparaffinized/rehydrated and then subjected to hematoxylin (Gill's formula; Vector Laboratories; catalog no. H3401) and eosin Y (Sigma-Aldrich; catalog no. E4009) (H&E) staining according to manufacturers' instructions.

Quantitative real-time PCR analysis. Lungs from *in vivo* experiments were isolated and homogenized in TRIzol prior to RNA extraction. DNase-treated total RNA was then reverse transcribed into cDNA using SuperScript II reverse transcriptase (Thermo Fisher) with oligo(dT) primers. Quantitative real-time PCR was performed using the Kapa Sybr Fast qPCR master mix kit (Kapa Biosystems) on a LightCycler 480 instrument II (Roche). Primers specific for *Isg15* (F, TCTATGAGGTCCGGCTGACA; R, GCACTGGGGCTTTAGGTCAT), *Irf7* (F, ATTTCGGTCGCAGGGATCTG; R, TGCAAGATAAAGCGTCCCGT), and *Actb* (F, CCAAGGCCAACCGTGAAAAG; R, ATGGCTACGTACATGGCTGG) were used. Delta-delta cycle threshold was determined relative to noninfected samples. Significance was determined using an unpaired two-tailed Student *t* test.

Transcriptome sequencing (RNA-Seq) analysis. Total RNA as described above was enriched for polyadenylated RNA and prepared for next-generation sequencing using the TruSeq Stranded mRNA library prep kit (Illumina), according to the manufacturer's instructions. Differential gene expression (DGE) between control groups and experimental groups was tested using a negative binomial model extended with quasilikelihood methods (QLF). All genes with a false-discovery rate (FDR) of <0.05 were classified as differentially expressed genes.

Statistical analysis. Significance was determined by two-way analysis of variance (ANOVA) followed by Tukey's test or Student's *t* test using Prism Software (GraphPad). A *P* value of <0.05 was considered significant.

Data availability. All RNA-Seq data obtained in this paper can be found on the NCBI Gene Expression Omnibus (GEO) under accession numbers GSE161200 and GSE203001.

ACKNOWLEDGMENT

We thank the Zegar Family Foundation for supporting this research.

REFERENCES

1. Wu F, Zhao S, Yu B, Chen YM, Wang W, Song ZG, Hu Y, Tao ZW, Tian JH, Pei YY, Yuan ML, Zhang YL, Dai FH, Liu Y, Wang QM, Zheng JJ, Xu L, Holmes EC, Zhang YZ. 2020. A new coronavirus associated with human respiratory disease in China. Nature 579:265–269. https://doi.org/10.1038/s41586-020-2008-3.

2. Zhu N, Zhang D, Wang W, Li X, Yang B, Song J, Zhao X, Huang B, Shi W, Lu R, Niu P, Zhan F, Ma X, Wang D, Xu W, Wu G, Gao GF, Tan W, China Novel Coronavirus Investigating and Research Team. 2020. A novel coronavirus from patients with pneumonia in China, 2019. N Engl J Med 382:727–733. https://doi.org/10.1056/NEJMoa2001017.
3. Carreño JM, Alshammary H, Tcheou J, Singh G, Raskin AJ, Kawabata H, Sominsky LA, Clark JJ, Adelsberg DC, Bielak DA, Gonzalez-Reiche AS, Dambrauskas N, Vigdorovich V, PSP-PARIS Study Group, Srivastava K, Sather DN, Sordillo EM, Bajic G, van Bakel H, Simon V, Krammer F. 2022. Activity of convalescent and vaccine serum against SARS-CoV-2 Omicron. Nature 602:682–688. https://doi.org/10.1038/d41586-021-03846-z.
4. Si L, Bai H, Rodas M, Cao W, Oh CY, Jiang A, Moller R, Hoagland D, Oishi K, Horiuchi S, Uhl S, Blanco-Melo D, Albrecht RA, Liu WC, Jordan T, Nilsson-Payant BE, Golynker I, Frere J, Logue J, Haupt R, McGrath M, Weston S, Zhang T, Plebani R, Soong M, Nurani A, Kim SM, Zhu DY, Benam KH, Goyal G, Gilpin SE, Prantil-Baun R, Gygi SP, Powers RK, Carlson KE, Frieman M, tenOever BR, Ingber DE. 2021. A human-airway-on-a-chip for the rapid identification of candidate antiviral therapeutics and prophylactics. Nat Biomed Eng 5:815–829. https://doi.org/10.1038/s41551-021-00718-9.
5. Ho JSY, Mok BW-Y, Campisi L, Jordan T, Yildiz S, Parameswaran S, Wayman JA, Gaudreault NN, Meekins DA, Indran SV, Morozov I, Trujillo JD, Fstkchyan YS, Rathnasinghe R, Zhu Z, Zheng S, Zhao N, White K, Ray-Jones H, Malysheva V, Thiecke MJ, Lau S-Y, Liu H, Zhang AJ, Lee AC-Y, Liu W-C, Jangra S, Escalera A, Aydillo T, Melo BS, Guccione E, Sebra R, Shum E, Bakker J, Kaufman DA, Moreira AL, Carossino M, Balasuriya UBR, Byun M, Albrecht RA, Schotsaert M, Garcia-Sastre A, Chanda SK, Miraldi ER, Jeyasekharan AD, TenOever BR, Spivakov M, Weirauch MT, Heinz S, Chen H, Benner C, Richt JA, Marazzi I. 2021. TOP1 inhibition therapy protects against SARS-CoV-2-induced lethal inflammation. Cell 184:2618–2632.e17. https://doi.org/10.1016/j.cell.2021.03.051.
6. Hou YJ, Okuda K, Edwards CE, Martinez DR, Asakura T, Dinnon KH, III, Kato T, Lee RE, Yount BL, Mascenik TM, Chen G, Olivier KN, Ghio A, Tse LV, Leist SR, Gralinski LE, Schafer A, Dang H, Gilmore R, Nakano S, Sun L, Fulcher ML, Livraghi-Butrico A, Nicely NI, Cameron M, Cameron C, Kelvin DJ, de Silva A, Margolis DM, Markmann A, Bartelt L, Zumwalt R, Martinez FJ, Salvatore SP, Borczuk A, Tata PR, Sontake V, Kimple A, Jaspers I, O'Neal WK, Randell SH, Boucher RC, Baric RS. 2020. SARS-CoV-2 reverse genetics reveals a variable infection gradient in the respiratory tract. Cell 182:429–446.e14. https://doi.org/10.1016/j.cell.2020.05.042.
7. Chen N, Zhou M, Dong X, Qu J, Gong F, Han Y, Qiu Y, Wang J, Liu Y, Wei Y, Xia J, Yu T, Zhang X, Zhang L. 2020. Epidemiological and clinical characteristics of 99 cases of 2019 novel coronavirus pneumonia in Wuhan, China: a descriptive study. Lancet 395:507–513. https://doi.org/10.1016/S0140-6736(20)30211-7.
8. Blanco-Melo D, Nilsson-Payant BE, Liu WC, Uhl S, Hoagland D, Moller R, Jordan TX, Oishi K, Panis M, Sachs D, Wang TT, Schwartz RE, Lim JK, Albrecht RA, tenOever BR. 2020. Imbalanced host response to SARS-CoV-2 drives development of COVID-19. Cell 181:1036–1045.e9. https://doi.org/10.1016/j.cell.2020.04.026.
9. Rydyznski Moderbacher C, Ramirez SI, Dan JM, Grifoni A, Hastie KM, Weiskopf D, Belanger S, Abbott RK, Kim C, Choi J, Kato Y, Crotty EG, Kim C, Rawlings SA, Mateus J, Tse LPV, Frazier A, Baric R, Peters B, Greenbaum J, Ollmann Saphire E, Smith DM, Sette A, Crotty S. 2020. Antigen-specific adaptive immunity to SARS-CoV-2 in acute COVID-19 and associations with age and disease severity. Cell 183:996–1012.e19. https://doi.org/10.1016/j.cell.2020.09.038.
10. Takahashi T, Yale IMPACT Research Team, Ellingson MK, Wong P, Israelow B, Lucas C, Klein J, Silva J, Mao T, Oh JE, Tokuyama M, Lu P, Venkataraman A, Park A, Liu F, Meir A, Sun J, Wang EY, Casanovas-Massana A, Wyllie AL, Vogels CBF, Earnest R, Lapidus S, Ott IM, Moore AJ, Yale IRT, Shaw A, Fournier JB, Odio CD, Farhadian S, Dela Cruz C, Grubaugh ND, Schulz WL, Ring AM, Ko AI, Omer SB, Iwasaki A. 2020. Sex differences in immune responses that underlie COVID-19 disease outcomes. Nature 588:315–320. https://doi.org/10.1038/s41586-020-2700-3.
11. de Jesus RP, de Carvalho JF, de Oliveira LPM, Cunha CM, Alves T, Vieira STB, Figueiredo VM, Bueno AA. 2022. Metabolic and nutritional triggers associated with increased risk of liver complications in SARS-CoV-2. World J Hepatol 14:80–97. https://doi.org/10.4254/wjh.v14.i1.80.
12. Lee JH, Koepke L, Kirchhoff F, Sparrer KMJ. 2022. Interferon antagonists encoded by SARS-CoV-2 at a glance. Med Microbiol Immunol https://doi.org/10.1007/s00430-022-00734-9.
13. Byrd KM, Beckwith CG, Garland JM, Johnson JE, Aung S, Cu-Uvin S, Farmakiotis D, Flanigan T, Gillani FS, Macias-Gil R, Mileno M, Ramratnam B, Rybak NR, Sanchez M, Tashima K, Mylonakis E, Kantor R. 2020. SARS-CoV-2 and HIV coinfection: clinical experience from Rhode Island, United States. J Int AIDS Soc 23:e25573. https://doi.org/10.1002/jia2.25573.
14. Nomah DK, Reyes-Uruena J, Llibre JM, Ambrosioni J, Ganem FS, Miro JM, Casabona J. 2022. HIV and SARS-CoV-2 co-infection: epidemiological, clinical features, and future implications for clinical care and public health for people living with HIV (PLWH) and HIV most-at-risk groups. Curr HIV/AIDS Rep 19:17–25. https://doi.org/10.1007/s11904-021-00596-5.
15. Lin Y, Yuan J, Long Q, Hu J, Deng H, Zhao Z, Chen J, Lu M, Huang A. 2021. Patients with SARS-CoV-2 and HBV co-infection are at risk of greater liver injury. Genes Dis 8:484–492. https://doi.org/10.1016/j.gendis.2020.11.005.
16. Leon FJF, da Silva LL, Santos AC, Duarte da Costa V, Miguel JC, Marques JT, Nascimento GP, Ferreira da Silva E, Lewis-Ximenez LL, Villar LM, de Paula VS. 2022. Immunological and virological aspects of severe acute respiratory syndrome coronavirus 2 (SARS-CoV-2) and hepatitis C virus. J Med Virol 94:2296–2301. https://doi.org/10.1002/jmv.27614.
17. Yue H, Zhang M, Xing L, Wang K, Rao X, Liu H, Tian J, Zhou P, Deng Y, Shang J. 2020. The epidemiology and clinical characteristics of co-infection of SARS-CoV-2 and influenza viruses in patients during COVID-19 outbreak. J Med Virol 92:2870–2873. https://doi.org/10.1002/jmv.26163.
18. Lew S, Manes P, Smith B. 2020. Coinfection with SARS-CoV-2 and influenza A virus in a 32-year-old man. Am J Case Rep 21:e926092. https://doi.org/10.12659/AJCR.926092.
19. Nowak MD, Sordillo EM, Gitman MR, Paniz Mondolfi AE. 2020. Coinfection in SARS-CoV-2 infected patients: where are influenza virus and rhinovirus/enterovirus? J Med Virol 92:1699–1700. https://doi.org/10.1002/jmv.25953.
20. Dao TL, Hoang VT, Colson P, Million M, Gautret P. 2021. Co-infection of SARS-CoV-2 and influenza viruses: a systematic review and meta-analysis. J Clin Virol Plus 1:100036. https://doi.org/10.1016/j.jcvp.2021.100036.
21. Lansbury L, Lim B, Baskaran V, Lim WS. 2020. Co-infections in people with COVID-19: a systematic review and meta-analysis. J Infect 81:266–275. https://doi.org/10.1016/j.jinf.2020.05.046.
22. Hoffmann M, Kleine-Weber H, Schroeder S, Kruger N, Herrler T, Erichsen S, Schiergens TS, Herrler G, Wu NH, Nitsche A, Muller MA, Drosten C, Pohlmann S. 2020. SARS-CoV-2 cell entry depends on ACE2 and TMPRSS2 and is blocked by a clinically proven protease inhibitor. Cell 181:271–280.e8. https://doi.org/10.1016/j.cell.2020.02.052.
23. Weis W, Brown JH, Cusack S, Paulson JC, Skehel JJ, Wiley DC. 1988. Structure of the influenza virus haemagglutinin complexed with its receptor, sialic acid. Nature 333:426–431. https://doi.org/10.1038/333426a0.
24. Traylor ZP, Aeffner F, Davis IC. 2013. Influenza A H1N1 induces declines in alveolar gas exchange in mice consistent with rapid post-infection progression from acute lung injury to ARDS. Influenza Other Respir Viruses 7:472–479. https://doi.org/10.1111/j.1750-2659.2012.00414.x.
25. Govorkova EA, Murti G, Meignier B, de Taisne C, Webster RG. 1996. African green monkey kidney (Vero) cells provide an alternative host cell system for influenza A and B viruses. J Virol 70:5519–5524. https://doi.org/10.1128/JVI.70.8.5519-5524.1996.
26. Horiuchi S, Oishi K, Carrau L, Frere J, Moller R, Panis M, tenOever BR. 2021. Immune memory from SARS-CoV-2 infection in hamsters provides variant-independent protection but still allows virus transmission. Sci Immunol 6:eabm3131. https://doi.org/10.1126/sciimmunol.abm3131.
27. Emeny JM, Morgan MJ. 1979. Regulation of the interferon system: evidence that Vero cells have a genetic defect in interferon production. J Gen Virol 43:247–252. https://doi.org/10.1099/0022-1317-43-1-247.
28. Li Y, Renner DM, Comar CE, Whelan JN, Reyes HM, Cardenas-Diaz FL, Truitt R, Tan LH, Dong B, Alysandratos KD, Huang J, Palmer JN, Adappa ND, Kohanski MA, Kotton DN, Silverman RH, Yang W, Morrisey EE, Cohen NA, Weiss SR. 2021. SARS-CoV-2 induces double-stranded RNA-mediated innate immune responses in respiratory epithelial-derived cells and cardiomyocytes. Proc Natl Acad Sci U S A 118:e2022643118. https://doi.org/10.1073/pnas.2022643118.
29. Imai M, Iwatsuki-Horimoto K, Hatta M, Loeber S, Halfmann PJ, Nakajima N, Watanabe T, Ujie M, Takahashi K, Ito M, Yamada S, Fan S, Chiba S, Kuroda M, Guan L, Takada K, Armbrust T, Balogh A, Furusawa Y, Okuda M, Ueki H, Yasuhara A, Sakai-Tagawa Y, Lopes TJS, Kiso M, Yamayoshi S, Kinoshita N, Ohmagari N, Hattori SI, Takeda M, Mitsuya H, Krammer F, Suzuki T, Kawaoka Y. 2020. Syrian hamsters as a small animal model for SARS-CoV-2 infection and countermeasure development. Proc Natl Acad Sci U S A 117:16587–16595. https://doi.org/10.1073/pnas.2009799117.
30. Iwatsuki-Horimoto K, Nakajima N, Ichiko Y, Sakai-Tagawa Y, Noda T, Hasegawa H, Kawaoka Y. 2018. Syrian hamster as an animal model for the study of human influenza virus infection. J Virol 92:e01693-17. https://doi.org/10.1128/JVI.01693-17.
31. Hoagland DA, Moller R, Uhl SA, Oishi K, Frere J, Golynker I, Horiuchi S, Panis M, Blanco-Melo D, Sachs D, Arkun K, Lim JK, tenOever BR. 2021. Leveraging the antiviral type I interferon system as a first line of defense against SARS-CoV-2 pathogenicity. Immunity 54:557–570.e5. https://doi.org/10.1016/j.immuni.2021.01.017.

32. Frere JJ, Serafini RA, Pryce KD, Zazhytska M, Oishi K, Golynker I, Panis M, Zimering J, Horiuchi S, Hoagland DA, Møller R, Ruiz A, Overdevest JB, Kodra A, Canoll PD, Goldman JE, Borczuk AC, Chandar V, Bram Y, Schwartz R, Lomvardas S, Zachariou V, tenOever BR. 2022. SARS-CoV-2 infection results in lasting and systemic perturbations post recovery. bioRxiv. https://doi.org/10.1101/2022.01.18.476786.
33. Nilsson-Payant BE, Uhl S, Grimont A, Doane AS, Cohen P, Patel RS, Higgins CA, Acklin JA, Bram Y, Chandar V, Blanco-Melo D, Panis M, Lim JK, Elemento O, Schwartz RE, Rosenberg BR, Chandwani R, tenOever BR. 2021. The NF-κB transcriptional footprint is essential for SARS-CoV-2 replication. J Virol 95:e01257-21. https://doi.org/10.1128/JVI.01257-21.
34. Zheng X, Wang H, Su Z, Li W, Yang D, Deng F, Chen J. 2020. Co-infection of SARS-CoV-2 and influenza virus in early stage of the COVID-19 epidemic in Wuhan, China. J Infect 81:e128–e129. https://doi.org/10.1016/j.jinf.2020.05.041.
35. D'Abramo A, Lepore L, Palazzolo C, Barreca F, Liuzzi G, Lalle E, Nicastri E. 2020. Acute respiratory distress syndrome due to SARS-CoV-2 and influenza A co-infection in an Italian patient: mini-review of the literature. Int J Infect Dis 97:236–239. https://doi.org/10.1016/j.ijid.2020.06.056.
36. Fahim M, Ghonim H, Roshdy WH, Naguib A, Elguindy N, AbdelFatah M, Hassany M, Mohsen A, Afifi S, Eid A. 2021. Coinfection with SARS-CoV-2 and influenza A(H1N1) in a patient seen at an influenza-like illness surveillance site in Egypt: case report. JMIR Public Health Surveill 7:e27433. https://doi.org/10.2196/27433.
37. Hashemi SA, Safamanesh S, Ghasemzadeh-Moghaddam H, Ghafouri M, Azimian A. 2021. High prevalence of SARS-CoV-2 and influenza A virus (H1N1) coinfection in dead patients in Northeastern Iran. J Med Virol 93:1008–1012. https://doi.org/10.1002/jmv.26364.
38. Achdout H, Vitner EB, Politi B, Melamed S, Yahalom-Ronen Y, Tamir H, Erez N, Avraham R, Weiss S, Cherry L, Bar-Haim E, Makdasi E, Gur D, Aftalion M, Chitlaru T, Vagima Y, Paran N, Israely T. 2021. Increased lethality in influenza and SARS-CoV-2 coinfection is prevented by influenza immunity but not SARS-CoV-2 immunity. Nat Commun 12:5819. https://doi.org/10.1038/s41467-021-26113-1.
39. Bai L, Zhao Y, Dong J, Liang S, Guo M, Liu X, Wang X, Huang Z, Sun X, Zhang Z, Dong L, Liu Q, Zheng Y, Niu D, Xiang M, Song K, Ye J, Zheng W, Tang Z, Tang M, Zhou Y, Shen C, Dai M, Zhou L, Chen Y, Yan H, Lan K, Xu K. 2021. Coinfection with influenza A virus enhances SARS-CoV-2 infectivity. Cell Res 31:395–403. https://doi.org/10.1038/s41422-021-00473-1.
40. Halfmann PJ, Nakajima N, Sato Y, Takahashi K, Accola M, Chiba S, Fan S, Neumann G, Rehrauer W, Suzuki T, Kawaoka Y. 2022. SARS-CoV-2 interference of influenza virus replication in Syrian hamsters. J Infect Dis 225:282–286. https://doi.org/10.1093/infdis/jiab587.
41. Zhang AJ, Lee AC, Chan JF, Liu F, Li C, Chen Y, Chu H, Lau SY, Wang P, Chan CC, Poon VK, Yuan S, To KK, Chen H, Yuen KY. 2021. Coinfection by severe acute respiratory syndrome coronavirus 2 and influenza A(H1N1)pdm09 virus enhances the severity of pneumonia in golden Syrian hamsters. Clin Infect Dis 72:e978–e992. https://doi.org/10.1093/cid/ciaa1747.
42. Kim EH, Nguyen TQ, Casel MAB, Rollon R, Kim SM, Kim YI, Yu KM, Jang SG, Yang J, Poo H, Jung JU, Choi YK. 2022. Coinfection with SARS-CoV-2 and influenza A virus increases disease severity and impairs neutralizing antibody and CD4(+) T cell responses. J Virol 96:e0187321. https://doi.org/10.1128/jvi.01873-21.
43. Varble A, Albrecht RA, Backes S, Crumiller M, Bouvier NM, Sachs D, García-Sastre A, tenOever BR. 2014. Influenza A virus transmission bottlenecks are defined by infection route and recipient host. Cell Host Microbe 16:691–700. https://doi.org/10.1016/j.chom.2014.09.020.